JACS
JOURNAL OF THE AMERICAN CHEMICAL SOCIETY
Article
pubs.acs.org/JACS

Gold Nanocluster-Catalyzed Semihydrogenation: A Unique Activation Pathway for Terminal Alkynes

Gao Li and Rongchao Jin*

Department of Chemistry, Carnegie Mellon University, Pittsburgh, Pennsylvania 15213, United States

Supporting Information

ABSTRACT: We report high catalytic activity of ultrasmall spherical $Au_{25}(SC_2H_4Ph)_{18}$ and rod-shaped $Au_{25}(PPh_3)_{10}(C{\equiv}CPh)_5X_2$ (X = Br, Cl) nanoclusters supported on oxides for the semihydrogenation of terminal alkynes into alkenes with >99% conversion of alkynes and ~100% selectivity for alkenes. In contrast, internal alkynes cannot be catalyzed by such "ligand-on" Au_{25} catalysts; however, with "ligand-off" Au_{25} catalysts the internal alkynes can undergo semihydrogenation to yield *Z*-alkenes, similar to conventional gold nanoparticle catalysts. On the basis of the results, a unique activation pathway of terminal alkynes by "ligand-on" gold nanoclusters is identified, which should follow a deprotonation activation pathway via a R′—C≡C—$[Au_nL_m]$ (where L represents the protecting ligands on the cluster), in contrast with the activation mechanism on conventional gold nanocatalysts. This new activation mode is supported by observing the incorporation of deprotonated —C≡CPh as ligands on rod-shaped $Au_{25}(PPh_3)_{10}(C{\equiv}CPh)_5X_2$ nanoclusters under conditions similar to the catalytic reaction and by detecting the R′—C≡C—$[Au_n(SC_2H_4Ph)_m]$ via FT-IR spectroscopy.

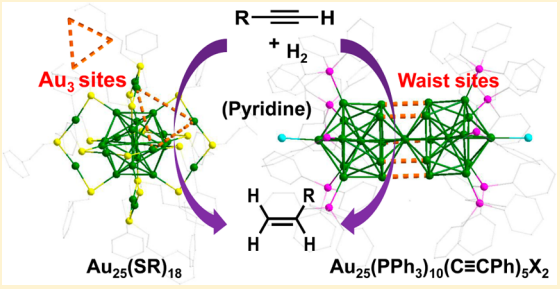

INTRODUCTION

The olefin (—C═C—) is typically synthesized by semihydrogenation of the alkyne functionality as a synthetic precursor, which is a common approach in organic synthesis.[1−3] In the previous catalytic approach, selective semihydrogenation of alkynes was catalyzed by palladium,[4−8] ruthenium,[9−11] iridium,[12] iron,[13] and nickel[14−17] complexes or nanoparticles. In recent research, nanogold catalysts have been reported to exhibit excellent catalytic performance in hydrogenation processes.[18−20] For the relatively large gold nanoparticles (>2 nm), Yan et al. reported the selective semihydrogenation of alkynes catalyzed by nanoporous gold using organosilanes with water as the hydrogen source, and the metallic Au(0) species was suggested to be the catalytic active sites in the hydrogenation reaction.[19] Ren et al. reported that TiO_2-supported gold nanoparticles (average size: ~3.5 nm) catalyzed selective hydrogenation of quinoline with H_2 as the reducing agent.[20]

Recently, atomically precise gold nanoclusters stimulated great interest in the catalytic hydrogenation.[21−24] For example, Zhu et al.[21] investigated the $Au_{25}(SR)_{18}$ (SR = thiolate) nanoclusters in both free and oxide-supported forms as catalysts for the chemoselective hydrogenation of *α,β*-unsaturated aldehydes and ketones in solution phase using H_2 gas as the reducing agent. Although the conversion of unsaturated aldehydes and ketones was not high enough (e.g., ~30%), the $Au_{25}(SR)_{18}$ catalyst remained intact after the hydrogenation process as the UV−vis spectrum of the $Au_{25}(SR)_{18}$ catalyst did not show noticeable changes after the hydrogenation reaction.[21] It was also reported that intact $Au_{25}(SR)_{18}$ and $Au_{25}(SG)_{18}$ (SG = glutathione) nanoclusters were effective in the reduction of 4-nitrophenol by $NaBH_4$.[22,23] In very recent work, we have investigated the catalytic performance of the free and oxide-supported $Au_n(SPh)_m$ nanoclusters (where n = 25, 36, and 99, m = 18, 24, and 42, respectively) in the chemoselective hydrogenation of reactants with nitro and aldehyde functional groups (e.g., nitrobenzaldehyde) into alcohols with the nitro group unaffected using H_2 gas as hydrogen resource;[24] indeed, the gold nanoclusters were found to be an excellent catalyst in the hydrogenation reactions.

The available crystal structure of the ultrasmall $Au_{25}(SR)_{18}$ nanocluster (1.27 nm metal core)[25] permits correlation of its reactivity with the atomic structure. The open facet of the $Au_{25}(SR)_{18}$ nanocluster exhibits a unique type of surface structure, that is, triangular gold sites (Au_3), for adsorbing and activating reactant molecules. For example, phenylacetylene (PhC≡CH) molecules could be adsorbed on the triangular Au_3 site on the open facet of the $Au_{25}(SR)_{18}$ nanocluster and then underwent the Sonogashira cross-coupling reaction.[26]

In this work, we report the oxide-supported spherical $Au_{25}(SR)_{18}$ and rod-shaped $Au_{25}(PPh_3)_{10}(C{\equiv}CPh)_5X_2$ (X = Cl, Br) nanocluster catalysts for the semihydrogenation of terminal alkynes to alkenes using H_2 as the hydrogen source under relatively mild conditions (100 °C, 20 bar H_2). To our knowledge, there has not been any report in the literature on the use of ultrasmall gold nanoclusters (1−2 nm) with *nonmetallic* electronic properties as catalysts for the semi-

Received: April 14, 2014
Published: July 30, 2014

dx.doi.org/10.1021/ja503724j | J. Am. Chem. Soc. 2014, 136, 11347−11354

hydrogenation process of alkynes, albeit ultrasmall gold nanocluster catalysts (e.g., $Au_{25}(SR)_{18}$ nanoclusters) have been reported for catalyzing other liquid-phase reaction process.[21−24,26−29] Importantly, a new alkyne-activation pathway is identified in the gold nanocluster-catalyzed semi-hydrogenation reaction.

■. RESULTS AND DISCUSSION

Characterization of the $Au_{25}(SR)_{18}/TiO_2$ Catalyst. The synthesis of $[Au_{25}(SR)_{18}]^-$ nanoclusters (counterion: tetraoctylammonium TOA^+, hereafter R = CH_2CH_2Ph) followed a previously reported method.[25] The oxide-supported nanocluster catalyst was made by impregnation of oxide powders (e.g., TiO_2, CeO_2, SiO_2, and Al_2O_3) in dichloromethane solution of $Au_{25}(SR)_{18}$ nanoclusters, followed by drying and annealing at 150 °C for 1 h in a vacuum oven; note that the free (i.e., unsupported) $Au_{25}(SR)_{18}$ nanoclusters are stable during the annealing treatment (even in air atmosphere).[26] We chose the $Au_{25}(SR)_{18}/TiO_2$ catalyst as an example for detailed characterization. The diffuse reflectance optical spectrum (400−1100 nm) of the $Au_{25}(SR)_{18}/TiO_2$ catalyst is shown in Figure 1A (black profile). The shorter-wavelength portion of the spectrum is dominated by the band gap absorption signal of TiO_2; of note, the band gap of TiO_2 is 3.0 eV (~410 nm). At longer wavelengths, a broad band from ~600 to 900 nm is seen in the diffuse reflectance spectrum of the catalyst, which is consistent with the solution optical spectrum of free $Au_{25}(SR)_{18}$ nanoclusters (Figure 1A, red profile). *Z*-contrast scanning transmission electron microscopy (STEM) analysis of the $Au_{25}(SR)_{18}/TiO_2$ catalyst shows that the size of gold nanoclusters (Figure 1B) remains to be 1.3 nm, consistent with the original size of monodisperse $Au_{25}(SR)_{18}$ nanoclusters.[30] Furthermore, thermogravimetric analysis (TGA) of the $Au_{25}(SR)_{18}/TiO_2$ catalyst also suggests that the protecting ligands are present on the gold nanoclusters.[26] All these results confirm that the $Au_{25}(SR)_{18}$ nanoclusters loaded on TiO_2 support did not decompose or grow to larger particles during the annealing process.

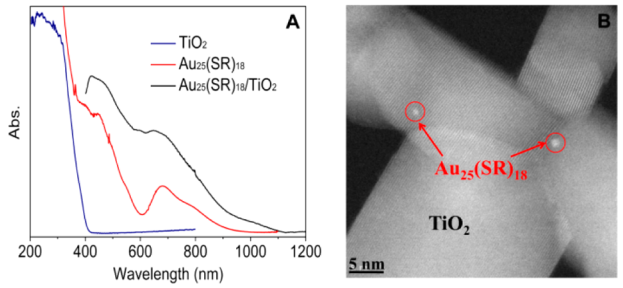

Figure 1. (A) Diffuse reflectance optical spectra of TiO_2 and $Au_{25}(SR)_{18}/TiO_2$, and solution-phase spectrum of free $Au_{25}(SR)_{18}$ nanoclusters (in dichloromethane). (B) STEM image of the $Au_{25}(SR)_{18}/TiO_2$ catalyst. Scale bar in panel B: 5 nm.

Thermal stability of the Free $Au_{25}(SR)_{18}$ Nanoclusters. To further confirm that the 150 °C annealing step does not alter the $Au_{25}(SR)_{18}$ nanoclusters, we performed a test of 150 °C thermal treatment of the unsupported $Au_{25}(SR)_{18}$ nanoclusters (in powders) in a vacuum oven for 1 h (i.e., the same as the supported $Au_{25}(SR)_{18}/TiO_2$ catalyst). Of note, the thiolate desorption temperature is above 200 °C.[30] We chose the unsupported $Au_{25}(SR)_{18}$ nanoclusters as they can be readily characterized by UV−vis, matrix-assisted laser desorption ionization mass spectrometry (MALDI−MS), and proton nuclear magnetic resonance (^1H NMR) spectroscopy. As shown in Figure 2A, the similar optical spectra before/after the

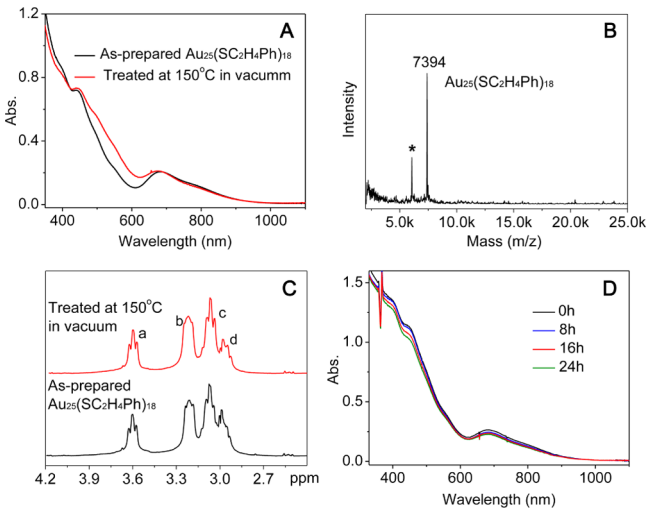

Figure 2. (A) UV−vis absorption spectra of the initial $[Au_{25}(SR)_{18}]^-$ (in dichloromethane) and the redissolved nanoclusters after thermal treatment of powders at 150 °C in a vacuum oven for 1 h. (B) Positive mode MALDI mass spectrum of $Au_{25}(SR)_{18}$ after thermal treatment, the peak marked with an asterisk (*) is a fragment caused by MALDI rather than an impurity. (C) ^1H NMR spectra (2.4 to 4.2 ppm range) of the $Au_{25}(SR)_{18}$ nanoclusters before and after the thermal treatment (powders dissolved in $CDCl_3$ for NMR measurements); the full range NMR spectra are shown in Figure S1 in the Supporting Information. (D) Thermal stability of $Au_{25}(SR)_{18}$ in a closed cuvette (dissolved in toluene, at 80 °C for 24 h).

treatment indicate that the $Au_{25}(SR)_{18}$ nanoclusters remain intact after the thermal treatment; of note, some of the $[Au_{25}(SR)_{18}]^-$ nanoclusters were transformed to $[Au_{25}(SR)_{18}]^0$, causing a slight change to the optical spectrum. Furthermore, MALDI−MS analysis (Figure 2B) of the thermally treated sample shows clean signals at m/z = 7394 (assigned to the molecular ion peak of $Au_{25}(SR)_{18}$, theoretical molecular weight: m/z = 7394); note that a fragment of $Au_{25}(SR)_{18}$ caused by MALDI was observed at 6057 (assigned to $Au_{21}(SR)_{14}$, after losing an $Au_4(SR)_4$ unit from the $Au_{25}(SR)_{18}$ nanocluster).[30] This fragment is inevitable in MALDI analysis and also exists in the analysis of the initial, pure $Au_{25}(SR)_{18}$ nanoclusters and, hence, does not indicate an impurity or decomposed product. No other peaks were found in wider range mass spectrometric analysis (e.g., from m/z 2000 up to 500k (k = 1000)), which means that no smaller or larger size gold nanoclusters were resulted after the thermal treatment of the $Au_{25}(SR)_{18}$ nanoclusters. Finally, the sample after thermal treatment was analyzed by NMR (Figure 2C). Compared to the NMR spectrum of the initial $Au_{25}(SR)_{18}$ (monoanionic, counterion = TOA^+) nanoclusters (Figure 2C, bottom profile), the thermally treated $Au_{25}(SR)_{18}$ nanoclusters show the same four proton peaks in the range from 2.4 to 4.2 ppm (Figure 2C, full-range spectra in Supporting Information Figure S1), which are from the four sets of methylene protons (i.e., inner and exterior types of $—CH_2CH_2Ph$ chemical environments in $Au_{25}(SR)_{18}$) as reported before.[31,32] Taken together, the $Au_{25}(SR)_{18}$ nanoclusters are thermally stable during the 150 °C annealing process. Furthermore, we tested the stability of the free $Au_{25}(SR)_{18}$ nanoclusters in toluene (solvent) at 80 °C (one of

dx.doi.org/10.1021/ja503724j | J. Am. Chem. Soc. 2014, 136, 11347−11354

Table 1. Optimization of Reaction Conditions for Semihydrogenation of 4-Phenyl-1-butyne Catalyzed by $Au_{25}(SR)_{18}/TiO_2$ Catalyst[a]

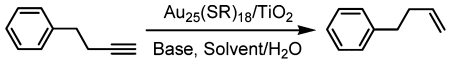

entry	T (°C)	solvent	base	conversion (%)[b]	selectivity (%)[b]
1	100	DMF	$NH_3 \cdot H_2O$	17.8	100
2	100	DMF	Et_2NH	21.6	100
3	100	DMF	Et_3N	3.9	100
4	100	DMF	Pyridine	61.7/63.8[c]	100
5	100	DMF	aniline	~100	26.4[d]
6	100	DMF	K_2CO_3	n.r.	
7	100	DMF	none	1.9	100
8	100	PhMe	Pyridine	15.2	100
9	100	MeCN	Pyridine	10.1	100
10	100	EtOH	Pyridine	~100	100
11	80	EtOH	Pyridine	36.0	100
12	60	EtOH	Pyridine	n.r.	

[a]Reaction conditions: 100 mg $Au_{25}(SR)_{18}/TiO_2$ catalyst (1 wt % loading of $Au_{25}(SR)_{18}$), 0.1 mmol 4-phenyl-1-butyne, 0.2 mmol base, 1 mL solvent:H_2O (10:1, V/V), 100 °C, 20 bar H_2, 20 h. [b]The conversion and selectivity were determined by ^1H NMR. [c]Isolated yield of 4-phenyl-1-butene. [d]The other product is 4-phenyl-2-butone and the selectivity is 73.6%. n.r. = no reaction.

the reaction temperatures, listed in Table 1) in a closed cuvette for 24 h. The process was monitored by recording the spectra at 8 h intervals; no sign of degradation was observed according to the superimposable spectra (Figure 2D).

Optimization of the Catalytic Semihydrogenation of Terminal Alkyne. With the $Au_{25}(SR)_{18}/TiO_2$ catalyst, we investigated the catalytic performance in semihydrogenation reaction and optimized the reaction conditions. The reaction was carried out under the following conditions: 0.1 mmol 4-phenyl-1-butyne, 0.2 mmol base, 1 mL solvent, and 100 mg TiO_2-supported $Au_{25}(SR)_{18}$ catalyst (~1 wt % loading of $Au_{25}(SR)_{18}$), 20 bar H_2, and 20 h (see details in the Experimental Section). The reaction product was analyzed by NMR spectroscopy (Figure S2 in the Supporting Information). Various combinations of solvent, base, and reaction temperature were tested for the semihydrogenation process. The initial result was quite promising; using ammonia as the base and DMF/H_2O mixture (10:1 V/V) as the solvent and temperature at 100 °C, 17.8% conversion (referring to alkyne, the same hereafter) was obtained (Table 1, entry 1). Other amines (secondary amine: diethylamine, tertiary amine: triethylamine and pyridine) were further examined (Table 1, entry 2–4); note that amine additives can largely promote the semihydrogenation reaction.[20] Among these amines, pyridine as the base gave the best catalytic result, that is, 61.7% conversion (Table 1, entry 4). There was no reaction when the base was changed to inorganic salt (K_2CO_3, Table 1, entry 6), and when no amine was present, only a 1.9% conversion was obtained (Table 1, entry 7). Primary amine (e.g., aniline) as the base has also been investigated (Table 1, entry 5), in which ~100% conversion of 4-phenyl-1-butyne was obtained, but the competing hydroamination process[33] occurred and the ketone product (i.e., 4-phenyl-2-butone) was formed in the crude products (selectivity for 4-phenyl-2-butone: 73.6%).

Further, other solvents (including protic solvent ethanol and aprotic solvents toluene and acetonitrile) were examined. The protic solvent (e.g., ethanol) gave an excellent catalytic result (~100% yield), which is much better than the aprotic solvents (Table 1, entry 10 vs entries 8 and 9). Finally, we investigated the temperature effect on the semihydrogenation. When the reaction temperature was decreased from 100 to 80 °C and further to 60 °C, the conversion was decreased from ~100% to 36% and to almost zero (Table 1, entry 10 vs entries 11 and 12). On the basis of the above optimizations, we chose ethanol/H_2O as the mixed solvent, pyridine as the base and reaction temperature of 100 °C as the optimized conditions for the semihydrogenation reaction.

Scope of the Catalytic Reaction: Terminal Alkynes. The catalytic activity of $Au_{25}(SR)_{18}/TiO_2$ was further examined with various terminal alkynes under the optimized reaction conditions. As shown in Table 2, the terminal chain alkynes (1-hexyne, 1-octyne, and 1-decyne) and terminal aromatic alkyne (phenylacetylene) all gave high conversion (>99%) and high selectivity for the product of alkene (~100%).

Support Effect. It is well known that the oxide supports of nanogold catalysts may have large influences on the catalytic

Table 2. Semihydrogenation of Terminal Alkynes at 100% Selectivity on $Au_{25}(SR)_{18}/TiO_2$ Catalyst[a]

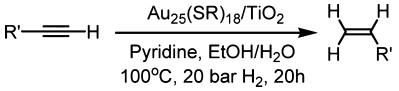

Entry	Alkyne	Alkene	Conv. [%]
1	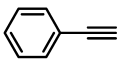	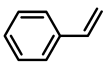	99.2
2	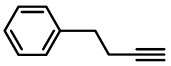	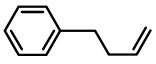	~100
3			99.5
4			99.6
5			99.4

[a]Reaction conditions: 100 mg $Au_{25}(SR)_{18}$(1 wt %)/TiO_2 catalyst, 0.1 mmol alkynes, 0.2 mmol pyridine, 1 mL EtOH:H_2O (10:1, V/V), 100 °C, 20 bar H_2, 20 h.

dx.doi.org/10.1021/ja503724j | J. Am. Chem. Soc. 2014, 136, 11347–11354

performance (e.g., conversion and selectivity).[34,35] In our system, blank experiments using gold-free TiO_2 gave no conversion under the same reaction conditions; thus, it clearly shows that the catalytic sites are associated with the Au nanocluster. To investigate the potential effect of the oxide supports, we compared four different oxides (i.e., CeO_2, SiO_2, TiO_2, and Al_2O_3) as supports for the $Au_{25}(SR)_{18}$ nanocluster. For all the investigated $Au_{25}(SR)_{18}$/oxide catalysts (Figure S3 in the Supporting Information), no obvious influence was observed in the catalytic performance of the semihydrogenation reaction of 4-phenyl-1-butyne, that is, all the catalysts gave high conversion and selectivity around 99%.

Recyclability of the $Au_{25}(SR)_{18}/TiO_2$ Catalyst. The catalytic performance of the recycled $Au_{25}(SR)_{18}/TiO_2$ catalyst was further investigated. In this test, the $Au_{25}(SR)_{18}/TiO_2$ catalyst was recovered simply by centrifugation after the semihydrogenation reaction; then, a new catalytic reaction was run under identical conditions except using the recycled catalyst. After five cycles, we only found a slight decrease in the conversion (within ~1%) (Figure S4 in the Supporting Information); thus, the catalyst has an excellent recyclability.

Pathway of the Terminal Alkyne Adsorption and Activation on Au_{25} Catalyst. The catalytic performance of $Au_{25}(SR)_{18}$ catalyst can be correlated with its atomic structure. The X-ray crystal structure of the $Au_{25}(SR)_{18}$ nanocluster[25] shows a 13-atom icosahedral Au_{13} core protected by six "—S(R)—Au—S(R)—Au—S(R)—" dimeric staple motifs (Figure 3A). On the two open facets (Figure 3B), three external

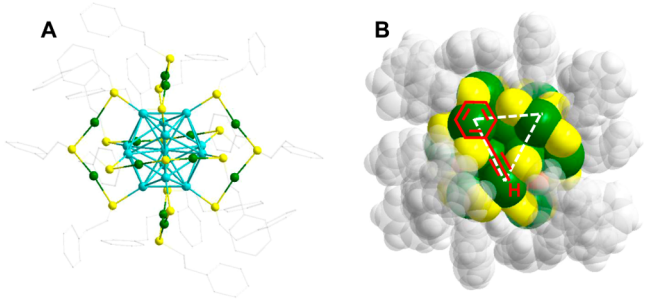

Figure 3. (A) The crystal structure of $Au_{25}(SR)_{18}$ nanoclusters.[25] (B) Scheme of the terminal alkyne molecule's initial adsorption on the surface of the $Au_{25}(SC_2H_4Ph)_{18}$ nanocluster.[26] The gold cluster is shown as the space-filling model, and phenylacetylene is used to represent the terminal alkynes. Color code: Au, green and cyan; S, yellow; C, gray; H, white.

gold atoms from the respective three adjacent staples constitutes a triangular Au_3 site, which is well exposed with less steric hindrance for reactant access. Previously, we theoretically studied the adsorption of phenylacetylene on the surface of $Au_{25}(SR)_{18}$ nanocluster.[26] Density functional theory (DFT) simulations indicated that the phenylacetylene molecule is adsorbed on the open Au_3 site with an adsorption energy of −0.40 eV.[26] In the initial adsorption configuration, the phenyl ring of phenylacetylene facing an external gold atom of the Au_3 site and the —C≡CH group of phenylacetylene points toward a second Au atom of the Au_3 site (Figure 3B); note that the third Au atom of the Au_3 site is unoccupied and thus can be used for hydrogen adsorption and activation facilitated by pyridine in the present semihydrogenation process.

With respect to the alkyne activation step in the semihydrogenation, the terminal alkyne (H—C≡C—R) can be activated by gold nanoparticles via two possible pathways: (1) the whole C≡C bond of the alkyne interacts with the surface of gold nanoparticle and becomes activated as discussed in previous work;[18−20] (2) the terminal of the C≡C bond (***H***—***C***≡C—R) interacts with gold and becomes activated. We are inclined to the second pathway, and the clue comes from the fact that terminal alkyne can ligate with the gold nanocluster surface as reported by Tsukuda and co-workers.[36−38] In their work, a series of alkyne-protected Au nanoclusters, such as $Au_{34}(C{\equiv}CPh)_{16}$, $Au_{54}(C{\equiv}CPh)_{26}$, $Au_{30}(EPT)_{13}$, and $Au_{35}(EPT)_{18}$ (EPT = 9-ethynyl-phenanthrene), have been synthesized; the protecting ligand (i.e., terminal alkynes) on the gold surface was exclusively deprotonated (i.e., R—C≡C—Au), which was also supported by DFT simulations.[39] Thus, the second pathway (i.e., deprotonation-induced activation) is most probable in the semihydrogenation catalyzed by $Au_{25}(SR)_{18}/TiO_2$. To gain further evidence, we added phenylacetylene to the $Au_{25}(SR)_{18}$ nanoclusters (in toluene solution) in the presence of excess pyridine under N_2 atmosphere at 80 °C for 4 h, similar to the reaction conditions in this work. Fourier-transform infrared (FT-IR) spectroscopic analysis identified the C≡C stretching peak at 2105 cm^{-1} (Figure 4), consistent with

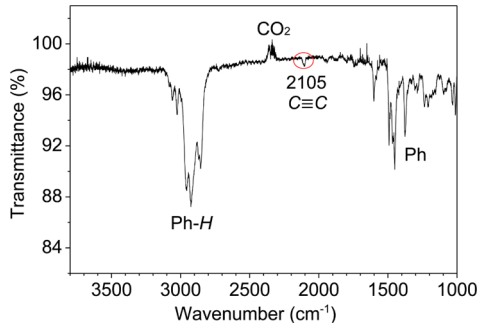

Figure 4. FT-IR spectrum of the Ph—C≡C···$[Au_{25}(SR)_{18}]$. The peak at ~2105 cm^{-1} belongs to *C*≡*C* stretching frequency.

the reported C≡C stretching frequency (~2124 cm^{-1}).[40,41] Further, there was no peak from 3400 to 3200 cm^{-1} (the range for C≡C—**H** stretch of free phenylacetylene), indicating that the semihydrogenation reaction catalyzed by $Au_{25}(SR)_{18}$ nanocluster proceeds via the second pathway, that is, the deprotonation-induced activation.

Catalytic Performance of the Au_{25} Catalyst in the Semihydrogenation of Internal Alkynes. To confirm the new activation pathway of terminal alkynes on $Au_{25}(SR)_{18}/TiO_2$, we chose internal alkynes to examine the catalytic activity of $Au_{25}(SR)_{18}/TiO_2$ catalyst under the aforementioned reaction conditions. It was found that the $Au_{25}(SR)_{18}/TiO_2$ catalyst showed no activity (i.e., all below 1%) in the reactions (Table 3, c.f. entry 1 vs 2−4); this agrees with the deprotonation activation mechanism of terminal alkynes because an internal alkyne has no terminal hydrogen and, thus, cannot be activated by the ultrasmall $Au_{25}(SR)_{18}$ nanoclusters according to the above deprotonation activation pathway.

Furthermore, we tested the *ligand-off* catalyst (Au_{25}/TiO_2), which was prepared by thermally treating the $Au_{25}(SR)_{18}/TiO_2$ powder at 300 °C (note: thiolate desorption onset: 200 °C[30]) for 1 h. With the bare Au_{25}/TiO_2 catalyst, the semihydrogenation reactions of internal alkynes (including 1-phenyl-1-propyne, diphenylacetylene, and methyl 2-nonynoate) were performed under the same reaction conditions (see notes

dx.doi.org/10.1021/ja503724j | J. Am. Chem. Soc. 2014, 136, 11347−11354

Table 3. Comparison of Conversion in Semihydrogenation Catalyzed by Ligand-On and Ligand-Off Catalysts[a]

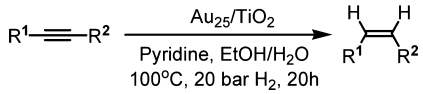

entry	catalyst	R^1	R^2	conversion	selectivity[b]
1	ligand-on Au_{25} sphere	PhC_2H_4	H	>99	
2		Ph	CH_3	<1	
3		Ph	Ph	<1	
4		n-C_6H_{13}	CO_2CH_3	<1	
5	ligand-off Au_{25}	PhC_2H_4	H	95.6	
6		Ph	CH_3	52.8	97
7		Ph	Ph	59.7	>99
8		n-C_6H_{13}	CO_2CH_3	52.6	99
9	ligand-on Au_{25} rod	PhC_2H_4	H	99.8	
10		Ph	CH_3	<1	
11		Ph	Ph	<1	
12		n-C_6H_{13}	CO_2CH_3	<1	

[a]Reaction conditions: as noted in Table 2. [b]Stereoselectivity for *Z*-alkene (see Figure S6 in the Supporting Information for the NMR spectra).

in Table 2). Interestingly, 52.6 to 59.7% conversions of internal alkynes with >97% stereoselectivity for *Z*-alkene were obtained (Table 3, entries 6–8), in striking contrast with the ligand-on $Au_{25}(SR)_{18}/TiO_2$ catalyst, which showed no activity (<1% conversion) in the reactions. Of note, the observed stereoselectivity over the ligand-off Au_{25}/TiO_2 catalyst is similar to the reported literature work in which conventional gold nanoparticles were used as the catalyst.[19] We also note that, similar to the ligand-on catalyst, the ligand-off Au_{25}/TiO_2 can catalyze the semihydrogenation of terminal alkynes, for example, 95.6% conversion of 4-phenyl-1-butyne (Table 3, entry 5).

The above catalytic results imply that the activation process of the terminal alkynes by $Au_{25}(SR)_{18}$ nanocluster catalyst is different than the cases by bare Au_{25} nanocluster and conventional gold nanoparticle catalysts. The activation of terminal alkynes by $Au_{25}(SR)_{18}$ nanocluster catalyst should occur through the terminal of the C≡C bond (***H***—***C***≡C—R′), and the constraint exerted by the ligand-on triangular Au_3 catalytic site apparently dictates this unique activation mode compared to the cases of bare nanoclusters and larger nanoparticles.

Comparison of Spherical and Rod-Shaped Au_{25} Nanoclusters. In order to confirm that the terminal alkynes can also ligate with gold nanoclusters protected by other ligands, rather than only the thiolate-protected nanoclusters, we etched triphenylphosphine (PPh_3)-protected gold nanoclusters in the presence of excess phenylacetylene (PhC≡CH) and pyridine at 80 °C (similar to the catalytic reaction conditions in this work). A new monodisperse product–gold nanocluster protected by both PPh_3 and —C≡CPh ligands, was obtained (Figure 5) and determined to be $[Au_{25}(PPh_3)_{10}(C{\equiv}CPh)_5X_2]^{2+}$ (X = Br, Cl) by electrospray ionization mass spectrometry (ESI–MS) analysis (Figure 5B). In the zoom-in spectrum (Figure S5A in the Supporting Information), prominent peaks (labeled I to V) are observed in the range of m/z 4080 to 4140, and the spacing of the experimental isotopic patterns is 0.5 (Figure S5C and D in the Supporting Information), indicating that the molecular ions (I–V) are all 2+ charged. The peak assignment is as follows: peak I at m/z = 4083.7 to $[MBrCl]^{2+}$, (where M = $Au_{25}(PPh_3)_{10}(C{\equiv}CPh)_5$, theoretical m/z: 4084.0), peak II at m/z 4096.6 ($[MBrClNa]^{2+}$, theoretical m/z 4095.5), peak III at m/z 4106.7 ($[MBr_2]^{2+}$, theoretical m/z 4106.3), peak IV at m/z 4118.1 ($[MBr_2Na]^{2+}$, theoretical m/z 4117.3), and peak V at m/z 4129.7 ($[MBr_2Na_2]^{2+}$, theoretical m/z 4129.3), with the experimental isotopic patterns matching well with simulations (Figure S5C and D in the Supporting Information). These results indicate that the alkyne can also ligate with the phosphine-protected Au_{25} nanoclusters and the alkyne ligands are also deprotonated, consistent with the alkyne activation pathway on thiolated $Au_{25}(SR)_{18}$ nanoclusters. Additionally, the optical absorption spectrum of $Au_{25}(PPh_3)_{10}(C{\equiv}CPh)_5X_2$ nanoclusters (Figure 5A) shows three stepwise peaks at 350, 407, and 626 nm, similar to the peaks of the reported $Au_{25}(PPh_3)_{10}(SR)_5X_2$ nanocluster[42,43] (Figure 5A). The similarities in both the formula and optical spectrum imply that the newly obtained $Au_{25}(PPh_3)_{10}(C{\equiv}CPh)_5X_2$ nanocluster should possess a biicosahedral structure (Figure S5F in the Supporting Information) similar to the X-ray structure of the $Au_{25}(PPh_3)_{10}(SR)_5X_2$ nanocluster (Figure S5E in the Supporting Information).[42,43] In the biicosahedral structure, the Au_{25} rod is composed of two icosahedral Au_{13} units by sharing one common Au vertex, and ten phosphines coordinate to the two Au_5 pentagonal rings on the two ends of the rod, and two halides (Cl or Br) bind to the two apical Au atoms, and five deprotonated alkyne ligands should bridge the two Au_{13} icosahedra, resembling the thiolate ligands (Figure S5E and F in the Supporting Information).

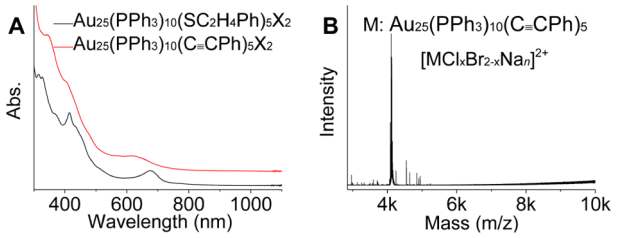

Figure 5. (A) Optical absorption spectra of $Au_{25}(PPh_3)_{10}(C{\equiv}CPh)_5X_2$ and $Au_{25}(PPh_3)_{10}(SC_2H_4Ph)_5X_2$ nanoclusters. The spectra are up-shifted for the ease of comparison. (B) Positive mode ESI-MS of the $Au_{25}(PPh_3)_{10}(C{\equiv}CPh)_5X_2$ (X = Cl/Br) nanoclusters.

Catalytic Property of Rod-Shaped Au_{25} Nanoclusters. The catalytic performance of the $Au_{25}(PPh_3)_{10}(C{\equiv}CPh)_5X_2$ nanocluster supported on TiO_2 (~1 wt % loading) was investigated. Using 4-phenyl-1-butyne as the reactant under the identical reaction conditions (Table 3, entry 9), a conversion of 99.8% with ~100% selectivity for the alkene product was obtained, but when using internal alkynes as the reactant, low catalytic activity was seen (Table 3, entries 10–12). These trends are similar to the case of the ligand-on $Au_{25}(SR)_{18}$ catalyst.

Mechanistic Insight. Taken together, the above catalytic results imply that the terminal alkyne activation should undergo a similar process over both types of ligand-on Au_{25} nanocluster catalysts. On the basis of the experimental results and the previous DFT calculations, we propose the following semihydrogenation mechanism (Figure 6). In the case of the spherical $Au_{25}(SR)_{18}$ nanocluster (Figure 6, left panel), the reactants (i.e., hydrogen and terminal alkyne (R′—C≡CH)) should be first absorbed on the open triangular Au_3 facet of the

dx.doi.org/10.1021/ja503724j | J. Am. Chem. Soc. 2014, 136, 11347–11354

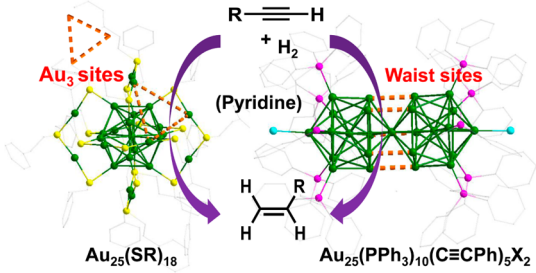

Figure 6. Proposed mechanism for the ligand-on Au_{25} nanocluster catalyzed semihydrogenation of terminal alkynes to alkenes using H_2 (20 bar). Left panel: $Au_{25}(SR)_{18}$ nanocluster.[25] Right panel: $Au_{25}(PPh_3)_{10}(C{\equiv}CPh)_5X_2$ (X = Cl, Br) nanocluster was drawn according to the crystal structure of the $Au_{25}(PPh_3)_{10}(SR)_5X_2$ nanocluster.[42,43] Color code: Au, green; S, yellow; C, gray; P, pink; X, cyan. Hydrogen atoms are omitted for clarity. The areas marked in orange are the Au_3 active sites (left panel) and the waist active sites (right panel) in the alkyne semihydrogenation reaction, respectively.

$Au_{25}(SR)_{18}$ nanocluster, and then the H—H bond and —C≡CH triple bond would be activated in the presence of a base (e.g., pyridine). Finally, the alkene product should be yielded after the addition process under the cooperation of three gold atoms of the Au_3 active site (Figure 6, left panel). In the case of the $Au_{25}(PPh_3)_{10}(C{\equiv}CPh)_5X_2$ rod cluster (Figure 6, right panel), the activation process of alkyne and the catalytic site of the semihydrogenation should be associated with the "waist" of the Au_{25} rod since the waist Au atoms should be bonded with the deprotonated alkynes (Figure S5F in the Supporting Information and Figure 6 right panel). The deprotonation activation of terminal alkyne (R′—C≡CH) and bridging adsorption of R′—C≡C on the catalytic site should be similar in both Au_{25} sphere and rod nanoclusters. This pathway is in contrast with the adsorption of alkynes on the "bare" Ru colloid, in which a type of Ru−vinylidene interfacial bond was formed.[44]

■. CONCLUSION

In summary, the catalytic performance of the spherical $Au_{25}(SR)_{18}$ and rod-shaped $Au_{25}(PPh_3)_{10}(C{\equiv}CPh)_5X_2$ nanoclusters (supported on oxides) have been investigated for the semihydrogenation of terminal alkynes to alkenes. High conversion of a range of terminal alkynes (up to ∼100%) with excellent selectivity (∼100%) for alkene products was achieved using ethanol/H_2O as the mixed solvent and pyridine as the base at 100 °C. No distinct effect of the oxide supports was observed. The nanocluster catalyst showed excellent recyclability. The open triangular Au_3 facet on the spherical $Au_{25}(SR)_{18}$ nanocluster and the waist sites of the rod-shaped $Au_{25}(PPh_3)_{10}(C{\equiv}CPh)_5X_2$ (X = Br/Cl) nanocluster are rationalized to be the active sites in the semihydrogenation process. In contrast with terminal alkynes, the internal alkynes cannot be catalyzed by the ligand-on nanoclusters, whereas the ligand-off nanoclusters are found to be capable of catalyzing the semihydrogenation of internal alkynes. Thus, a unique activation pathway is identified for terminal alkynes over ligand-on gold nanoclusters, and this mode is in contrast with the case of conventional gold nanoparticle catalysts. Specifically, the terminal alkynes should be activated via a R′—C≡C—$[Au_nL_m]$ (where L represents protecting ligands on the cluster) with clues from the incorporation of —C≡CPh in the $Au_{25}(PPh_3)_{10}(C{\equiv}CPh)_5X_2$ (X = Br/Cl) nanoclusters when PPh_3-protected Au nanoclusters are etched by phenylacetylene under similar conditions as in the catalytic reaction. The R′—C≡C—$[Au_n(SR)_m]$ was observed by FT-IR spectroscopy with the Au—**C≡C** stretching mode at 2105 cm^{-1}. Compared to conventional nanoparticles, the unique catalytic properties of nanoclusters are remarkable and such nanoclusters hold great promise in revealing the fundamental aspects of catalytic reactions.

■. EXPERIMENTAL SECTION

Chemicals. Tetrachloroauric(III) acid ($HAuCl_4{\cdot}3H_2O$, 99.99% metal basis, Aldrich), tetraoctylammonium bromide (TOAB, 98%, Fluka), sodium borohydride (99.99% trace metals basis, Aldrich), phenylethanethiol (98%, Sigma-Aldrich), triphenylphosphine (99%, Sigma-Aldrich), toluene (HPLC grade, 99.9%, Aldrich), methanol (absolute, 200 proof, Pharmco), methylene chloride (HPLC grade, 99.9%, Sigma-Aldrich), acetone (HPLC grade, 99.9%, Sigma-Aldrich), toluene (HPLC grade, 99.9%, Sigma-Aldrich), phenylacetylene (99%, Sigma-Aldrich), pyridine (99%, Sigma-Aldrich). All chemicals were used as received. Nanopure water (resistivity 18.2 MΩ·cm) was purified with a Barnstead NANOpure Diwater™ system. All glassware was thoroughly cleaned with aqua regia (HCl:HNO_3 = 3:1 v/v), rinsed with copious nanopure water, and then dried in an oven prior to use.

Thermal Stability Test of the Free $Au_{25}(SR)_{18}$ Nanoclusters. In this test, 4 mg of powders of $Au_{25}(SC_2H_4Ph)_{18}$ nanoclusters (monoanionic, counterion = tetraoctylammonium ion, TOA^+) was placed in a 5 mL tube and then annealed in a vacuum oven at 150 °C for ∼1 h. After that, the sample (dissolved in solution) was characterized by UV−vis, MALDI−MS, and ^1H NMR spectroscopy. UV−vis spectra of the clusters before/after annealing (dissolved in dicholomethane) were acquired on a Hewlett-Packard (HP) Agilent 8453 diode array spectrophotometer at room temperature. MALDI−MS was performed with a PerSeptiveBiosystems Voyager DE super-STR time-of-flight (TOF) mass spectrometer. Trans-2-[3-(4-*tert*-butylphenyl)-2-methyl-2-propenyldidene] malononitrile (DCTB) was used as the matrix in MALDI analysis. The nanoclusters and the matrix were disolved in dicholomethane and then spoted onto the steel plate and dried in vacumm prior to MALDI analysis. For NMR analysis, the $Au_{25}(SC_2H_4Ph)_{18}$ nanoclusters were dissolved in 0.5 mL $CDCl_3$ in a NMR tube and ^1H NMR was run on a Bruker 300 MHz spectrometer.

Identification of R′—C≡C—$[Au_n(SR)_m]$. $Au_{25}(SC_2H_4Ph)_{18}$ nanoclusters (1 mg) were dissolved in 1 mL of toluene, and then 100 μL of phenylacetylene and 90 μL of pyridine were added. The solution was heated to 80 °C under vigorous stirring and maintained at this temperature for 4 h (under a N_2 atmosphere). After that, the toluene was removed by rotary evaporation, and the left liquid was washed with hexane for six times to remove excess phenylacetylene and pyridine. Then the product was extracted by acetone, followed by centrifugation again to remove the insoluble components. Finally, the product was deposited onto a NaCl window by spotting a CH_2Cl_2 solution of the product, followed by FT-IR measurements on a Thermo/ATI/Mattson 60AR instrument (resolution, 1 cm^{-1}; scans, 16; range, 1000−4000 cm^{-1}).

Preparation of $Au_{25}(PPh_3)_{10}(C{\equiv}CPh)_5X_2$ (X = Cl, Br) Nanoclusters. $HAuCl_4{\cdot}3H_2O$ (78.8 mg, 0.2 mmol) and tetraoctylammonium bromide (TOAB, 131.3 mg, 0.24 mmol) were dissolved in 15 mL of acetone in a trineck round-bottom flask. After the solution was vigorously stirred for 10 min, PPh_3

dx.doi.org/10.1021/ja503724j | J. Am. Chem. Soc. 2014, 136, 11347−11354

(78.6 mg, 0.3 mmol) was added. The solution became colorless after 20 min. Then, $NaBH_4$ (22.8 mg, 0.6 mmol, dissolved in 5 mL ethanol) was added all at once. The solution immediately turned dark. The reaction was allowed to proceed for 2 h under air environment at room temperature. The crude black product (containing PPh_3-protected Au nanoparticles) was collected after rotary evaporation of the solvent. The black product was washed several times with hexane to remove excess PPh_3 and TOAB. The precipitated product was extracted by acetone, followed by centrifugation again to remove insoluble components. The left solution of Au nanoparticles was dried by rotary evaporation, and the solids were dissolved in 0.2 mL of phenylacetylene and 0.2 of mL pyridine. The solution was vigorously stirred at 80 °C for 4 h. The products were obtained after drying the solution by rotary evaporation and washing with hexane and finally extraction with methanol.

Preparation of $Au_{25}(SR)_{18}$/Oxide and Ligand-off Au_{25}/TiO_2 Catalysts. Typically, 1 mg of $Au_{25}(SR)_{18}$ nanoclusters were dissolved in 5 mL of dicholomethane, and 100 mg of oxide (e.g., CeO_2, TiO_2, Al_2O_3, or SiO_2) was added. After stirring for 12 h at rt, the $Au_{25}(SR)_{18}$/oxide catalysts were collected by centrifugation and dried in a vacuum. The catalysts were then annealed at 150 °C for ∼1 h in a vacuum oven. When the annealing temperature was increased to 300 °C, the thiolate ligands were desorbed and ligand-off Au_{25}/TiO_2 catalyst was obtained. No apparent particle size growth was observed in STEM analysis.

Typical Procedure for the Semihydrogenation Reaction. In a typical semihydrogenation reaction, alkyne (0.1 mmol), base (0.2 mmol), $Au_{25}(SR)_{18}$/oxide (100 mg, 1 wt % loading of $Au_{25}(SR)_{18}$) and 1 mL of solvent were added to a reactor (Parr Instrument Company, 22 mL capacity, series 4700) and H_2 was introduced until 20 bar. The reaction was kept at 100 °C for 20 h as indicated in Table 1. The product was obtained after removal of solvent. Both the conversion of alkyne and the selectivity for alkene were determined by ^1H NMR analysis.

■ ASSOCIATED CONTENT

Ⓢ Supporting Information

Full NMR analysis of the free $Au_{25}(SC_2H_4Ph)_{18}$ nanoclusters before and after annealing, testing of the support effects and recyclability of $Au_{25}(SC_2H_4Ph)_{18}$ nanocluster catalysts, experimental and simulated isotopic distribution patterns of $[Au_{25}(PPh_3)_{10}(C{\equiv}CPh)_5X_2]^{2+}$ (X = Cl, Br) nanoclusters, and data of ^1H NMR. This material is available free of charge via the Internet at http://pubs.acs.org.

■ AUTHOR INFORMATION

Corresponding Author

rongchao@andrew.cmu.edu.

Notes

The authors declare no competing financial interest.

■ ACKNOWLEDGMENTS

This work is financially supported by U. S. Department of Energy, Office of Basic Energy Sciences (Grant DE-FG02-12ER16354). We thank Prof Yu Lei for assistance with STEM imaging.

■ REFERENCES

(1) Oger, C.; Balas, L.; Durand, T.; Galano, J. *Chem. Rev.* **2013**, *113*, 1313−1350.
(2) Fürstner, A.; Davies, P. W. *Chem. Commun.* **2005**, *41*, 2307−2320.
(3) Michaelides, I. N.; Dixon, D. J. *Angew. Chem., Int. Ed.* **2013**, *52*, 806−808.
(4) Mitsudome, T.; Takahashi, Y.; Ichikawa, S.; Mizugaki, T.; Jitsukawa, K.; Kaneda, K. *Angew. Chem., Int. Ed.* **2013**, *52*, 1481−1485.
(5) Hauwert, P.; Maestri, G.; Sprengers, J. W.; Catellani, M.; Elsevier, C. J. *Angew. Chem., Int. Ed.* **2008**, *47*, 3223−3226.
(6) Shen, R.; Chen, T.; Zhao, Y.; Qiu, R.; Zhou, Y.; Yin, S.; Wang, X.; Goto, M.; Han, L. *J. Am. Chem. Soc.* **2011**, *133*, 17037−17044.
(7) Shirakawa, E.; Otsuka, H.; Hayashi, T. *Chem. Commun.* **2005**, *41*, 5885−5886.
(8) Li, J.; Hua, R.; Liu, T. *J. Org. Chem.* **2010**, *75*, 2966−2970.
(9) Belger, C.; Neisius, N. M.; Plietker, B. *Chem.—Eur. J.* **2010**, *16*, 12214−12220.
(10) Trost, B. M.; Ball, Z. T.; Jöge, T. *J. Am. Chem. Soc.* **2002**, *124*, 7922−7923.
(11) Li, J.; Hua, R. *Chem.—Eur. J.* **2011**, *17*, 8462−8465.
(12) Tani, K.; Iseki, A.; Yamagata, T. *Chem. Commun.* **1999**, *35*, 1821−1822.
(13) Belger, C.; Plietker, B. *Chem. Commun.* **2012**, *48*, 5419−5421.
(14) Barrios-Francisco, R.; García, J. J. *Appl. Catal. A: Gen.* **2010**, *385*, 108−113.
(15) Carenco, S.; Leyva-Pérez, A.; Concepción, P.; Boissière, C.; Mézailles, N.; Sanchez, C.; Corma, A. *Nano Today* **2012**, *7*, 21−28.
(16) Witte, P. T.; Boland, S.; Kirby, F.; van Maanen, R.; Bleeker, B. F.; de Winter, D. A. M.; Post, J. A.; Geus, J. W.; Berben, P. H. *ChemCatChem* **2013**, *5*, 582−587.
(17) Chung, J.; Kim, C.; Jeong, H.; Yu, T.; Binh, D. H.; Jang, J.; Lee, J.; Kim, B. M.; Lim, B. *Chem.—Asian J.* **2013**, *8*, 919−925.
(18) Arcadi, A. *Chem. Rev.* **2008**, *108*, 3266−3325.
(19) Yan, M.; Jin, T.; Ishikawa, Y.; Minato, T.; Fujita, T.; Chen, L.; Bao, M.; Asao, N.; Chen, M.; Yamamoto, Y. *J. Am. Chem. Soc.* **2012**, *134*, 17536−17542.
(20) Ren, D.; He, L.; Yu, L.; Ding, R.; Liu, Y.; Cao, Y.; He, H.; Fan, K. *J. Am. Chem. Soc.* **2012**, *134*, 17592−17598.
(21) Zhu, Y.; Qian, H.; Drake, B. A.; Jin, R. *Angew. Chem., Int. Ed.* **2010**, *49*, 1295−1298.
(22) Shivhare, A.; Ambrose, S. J.; Zhang, H.; Purves, R. W.; Scot, R. W. J. *Chem. Commun.* **2013**, *49*, 276−278.
(23) Yamamoto, H.; Yano, H.; Kouchi, H.; Obora, Y.; Arakawa, R.; Kawasaki, H. *Nanoscale* **2012**, *4*, 4148−4154.
(24) Li, G.; Zeng, C.; Jin, R. *J. Am. Chem. Soc.* **2014**, *136*, 3673−3679.
(25) Zhu, M.; Aikens, C. M.; Hollander, F. J.; Schatz, G. C.; Jin, R. *J. Am. Chem. Soc.* **2008**, *130*, 5883−5885.
(26) Li, G.; Jiang, D.; Liu, C.; Yu, C.; Jin, R. *J. Catal.* **2013**, *306*, 177−183.
(27) Li, G.; Jin, R. *Acc. Chem. Res.* **2013**, *46*, 1749−1758.
(28) Liu, J.; Krishna, K. S.; Losovyj, Y. B.; Chattopadhyay, S.; Lozova, N.; Miller, J. T.; Spivey, J. J.; Kumar, C. *Chem.—Eur. J.* **2013**, *19*, 10201−10208.
(29) Li, G.; Liu, C.; Lei, Y.; Jin, R. *Chem. Commun.* **2012**, *48*, 12005−12007.
(30) Qian, H.; Zhu, M.; Wu, Z.; Jin, R. *Acc. Chem. Res.* **2012**, *45*, 1470−1479.
(31) Liu, Z.; Zhu, M.; Meng, X.; Xu, G.; Jin, R. *J. Phys. Chem. Lett.* **2011**, *2*, 2104−2109.
(32) Qian, H.; Zhu, M.; Gayathri, C.; Gil, R. R.; Jin, R. *ACS Nano* **2011**, *5*, 8935−8942.
(33) Corma, A.; Concepcion, P.; Dominguez, I.; Fornes, V.; Sabater, M. J. *J. Catal.* **2007**, *251*, 39−47.
(34) Haruta, M. *CATTECH* **2002**, *6*, 102−115.
(35) Makosch, M.; Sá, J.; Kartusch, C.; Richner, G.; van Bokhoven, J. A.; Hungerbühler, K. *ChemCatChem* **2012**, *4*, 59−63.
(36) Maity, P.; Tsunoyama, H.; Yamauchi, M.; Xie, S.; Tsukuda, T. *J. Am. Chem. Soc.* **2011**, *133*, 20123−20125.

(37) Maity, P.; Wakabayashi, T.; Ichikuni, N.; Tsunoyama, H.; Xie, S.; Yamauchi, M.; Tsukuda, T. *Chem. Commun.* **2012**, *48*, 6085−6087.
(38) Maity, P.; Takano, S.; Yamazoe, S.; Wakabayashi, T.; Tsukuda, T. *J. Am. Chem. Soc.* **2013**, *135*, 9450−9457.
(39) Nykänen, L.; Häkkinen, H.; Honkala, K. *Carbon* **2012**, *50*, 2752−2763.
(40) Kilpin, K. J.; Horvath, R.; Jameson, G. B.; Telfer, S. G.; Gordon, K. C.; Crowley, J. D. *Organometallics* **2010**, *29*, 6186−6195.
(41) Chen, W.; Zuckerman, N. B.; Kang, X.; Ghosh, D.; Konopelski, J. P.; Chen, S. *J. Phys. Chem. C* **2010**, *114*, 18146−18152.
(42) Shichibu, Y.; Negishi, Y.; Watanabe, T.; Chaki, N. K.; Kawaguchi, H.; Tsukuda, T. *J. Phys. Chem. C* **2007**, *111*, 7845−7847.
(43) Qian, H.; Eckenhoff, W. T.; Bier, M. E.; Pintauer, T.; Jin, R. *Inorg. Chem.* **2011**, *50*, 10735−10739.
(44) Kang, X.; Zuckerman, N. B.; Konopelski, J. P.; Chen, S. *J. Am. Chem. Soc.* **2012**, *134*, 1412−1415.